PROCEEDINGS, 47th Workshop on Geothermal Reservoir Engineering
Stanford University, Stanford, California, February 7-9, 2022
SGP-TR-223

Geothermal Prospect Imaging through Joint Airborne ZTEM and Ground Magnetotelluric Data Inversion Analysis

Phil Wannamaker[1], Virginie Maris and Jean Legault

[1]University of Utah/Energy & Geoscience Institute, 423 Wakara Way, Suite 300, Salt Lake City, UT 84108, U.S.A.

pewanna@egi.utah.edu

Keywords: Airborne EM, ZTEM, Magnetotellurics, Inversion, Fault Zones, Fluids

ABSTRACT

Electromagnetic (EM) geophysical methods have been a priority technology in both enhanced geothermal systems (EGS) and hydrothermal exploration for imaging fluids, permeable pathways, and controlling structures. Natural EM field methods are the only practical option for probing depths of 2 km or more for geothermal resources. A DOE/GTO exploration R&D priority has been to develop an MT/EM/AFMAG airborne system capable of exploring to 2 km or more. Such a platform could cover large ground areas with high sampling density. The ZTEM (TM) airborne platform is simply MT tipper estimation with the vertical field sensor towed behind a helicopter and with the horizontal coils at a fixed ground location; it is otherwise processed and modeled similarly. Utilizing only the magnetic field, however, ZTEM requires an assumption for the host resistivity to correctly estimate body position and properties. Sparse MT sites in principle can help to resolve this, and the concept is largely validated in our experience. However, a consideration is the necessity to mobilize two survey types and to develop algorithms for the joint interpretation.

1. INTRODUCTION

A research goal of DOE/GTO has been to achieve detailed electrical resistivity resolution at geothermal reservoir scales by combining airborne natural electromagnetic (EM) field surveying (ZTEM) with ground magnetotelluric (MT) measurements to approximate an airborne MT geophysical method (Phillips et al., 2013; Ziagos et al., 2013). MT alone is relatively expensive and may have permitting challenges. Airborne ZTEM field data contains only the magnetic field, requires a background resistivity assumption, and has been limited to relatively high frequencies, thus suffering non-uniqueness. Based on prototype two-dimensional (2D) simulations presented herein, ZTEM ambiguities may be reduced through formal incorporation with sparse ground MT soundings. This is demonstrated on donated field data sets, first for a relatively 2D mining prospect and then in 3D for the Eleven Mile Canyon geothermal prospect.

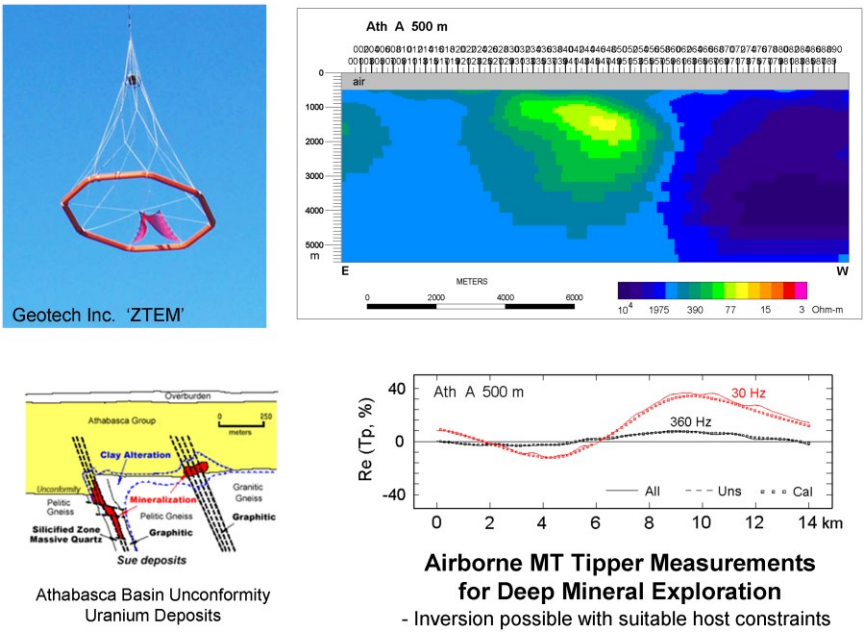

Figure 1: Picture of ZTEM vertical H-field sensor (upper left), 2D inversion image produced by flown profile data over the Athabasca Basin (upper right), schematic of unconformity uranium deposit (lower left), and fit of the inversion model calculations to the data for two frequencies of the survey (lower right). A background resistivity of 1000 ohm-m was assumed based on experience in the Athabascan environment. Data for inversion provided by Geotech Inc.

The ZTEM airborne platform (Figure 1) is simply MT tipper estimation with the vertical field sensor towed by helicopter and with the horizontal coils at a fixed ground location (Legault et al., 2009). ZTEM is as rigorous in its basis as traditional tipper, and is processed and modeled similarly. Utilizing only the magnetic field, however, ZTEM must assume a host resistivity to constrain body position and properties. Sparse MT sites in principle can resolve this, as we show with synthetic and field examples.

With MT data, on the other hand, inclusion of the electric field to define the tensor MT impedance brings intrinsic depth resolution without, in principle, external constraints on the host (Chave and Jones, 2012). We apply uniquely powerful 3D MT imaging capability based on deformable edge finite elements (FE) handling large topographic variations accurately, incorporating precise direct solvers throughout, and parallelized on single-box, multi-core, large-RAM workstations (HexMT code; Kordy et al., 2016a,b). Stair-step approximations to topography inherent to finite difference algorithms (Newman and Alumbaugh, 2000; Siripunvaraporn et al., 2005; Holtham and Oldenburg, 2010; Kelbert et al., 2014; Lee et al., 2018) are prone to E-field instabilities due to sharp cell corners. We compute million-parameter tomography problems with a direct data-space parameter formulation, as exemplified in Kordy et al., 2016a,b). Several additional MT field examples using this algorithm appear in Wannamaker et al. (2017, 2019, 2021).

2. BASIS FOR COMBINING AIRBORNE ZTEM WITH SPARSE GROUND MT

Two-dimensional computer simulation and inversion of coincident field data suggests that adding even very sparse MT soundings to a ZTEM survey will go far in resolving non-uniqueness and in approaching an airborne MT surveying technique. Figure 2 demonstrates this in 2D for both synthetic and field data models using our finite element inversion code (e.g., Wannamaker et al., 2008) augmented from that described by Legault et al. (2009). On the left in the figure, synthetic ZTEM data were at 7 frequencies from 720 Hz to 30 Hz. MT data were at 13 frequencies from 1000 Hz to 1 Hz. Field ZTEM and MT data were donated by Denison Mines Corp from the eastern Athabasca basin of Saskatchewan, Canada (Legault et al., 2009). With no MT included, an erroneous background assumption can yield images at the wrong depth. For both synthetic cases and real field data, adding just a few MT stations corrects both body position and background value from those initially resulting from incorrect back-ground assumptions. Inclusion of ZTEM H-field also may have improved lateral extent of conductive material at Johnston Lake. In the case with only 3 MT sites, the number of ZTEM data exceeded the MT by a factor of ~30. With some trial and error, we found that upweighting the MT data by about a factor of 4 yielded comparable misfits for the ZTEM and MT data, similar to Lee et al (2018). Nevertheless, the potential of joint sparse inversion to greatly improve resolution is clear, and should only be better in full 3D with topography as we have pursued here.

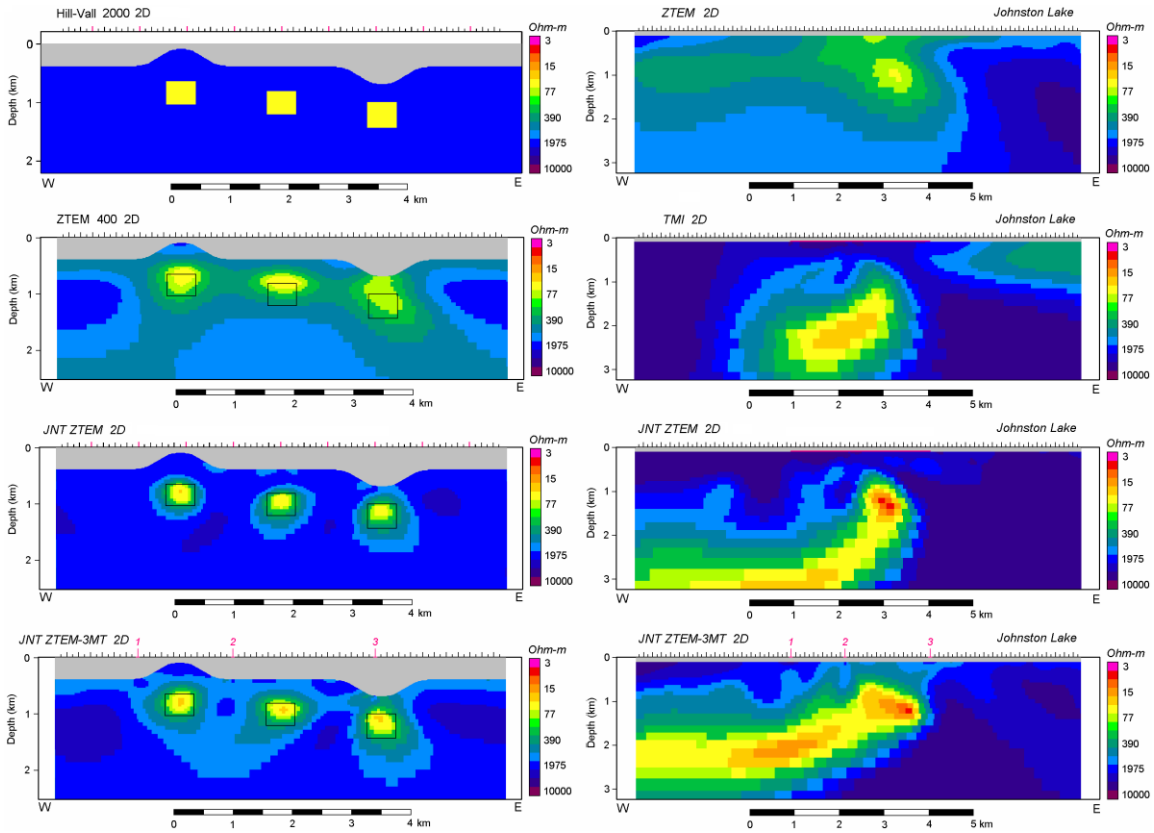

Figure 2: Joint MT/ZTEM 2D inversion examples. Left: 50 ohm-m bricks ~400 m deep in 2000 ohm-m host under hill and valley. Gray region is air with a draped bird flight height of 90 m. Second left panel is ZTEM-only inversion assuming 400 ohm-m host. Third panel left is joint MT-ZTEM inversion using all 9 MT sites (red ticks). Bottom left panel is inversion with only three MT sites. Right: Johnston Lake ZTEM profile of 198 sites with ZTEM-only inversion (top), TM mode MT array inversion only (second right), and ZTEM plus all MT sites (third right, TM mode), and only 3 MT sites for inversion (bottom right). Modified from Wannamaker and Legault (2014).

The algorithm next was exercised against a simple 3D synthetic structure (prism) to test image recovery (Figure 3). Gaussian error of 0.01 was added to the real and imaginary parts of the ZTEM response over five frequencies from 30 to 360 Hz at 3575 sites. An MT impedance error floor of 0.1*[|Zxy-Zyx|/2] was applied to synthetic data at quarter decade intervals from 1 Hz to 1000 Hz at 143 sites. The MT data were upweighted by a factor of 3 to balance influence. One sees that data fit convergence is rapid to just above unity and that the joint data image of the prism is definitely resolved better when both data sets are used.

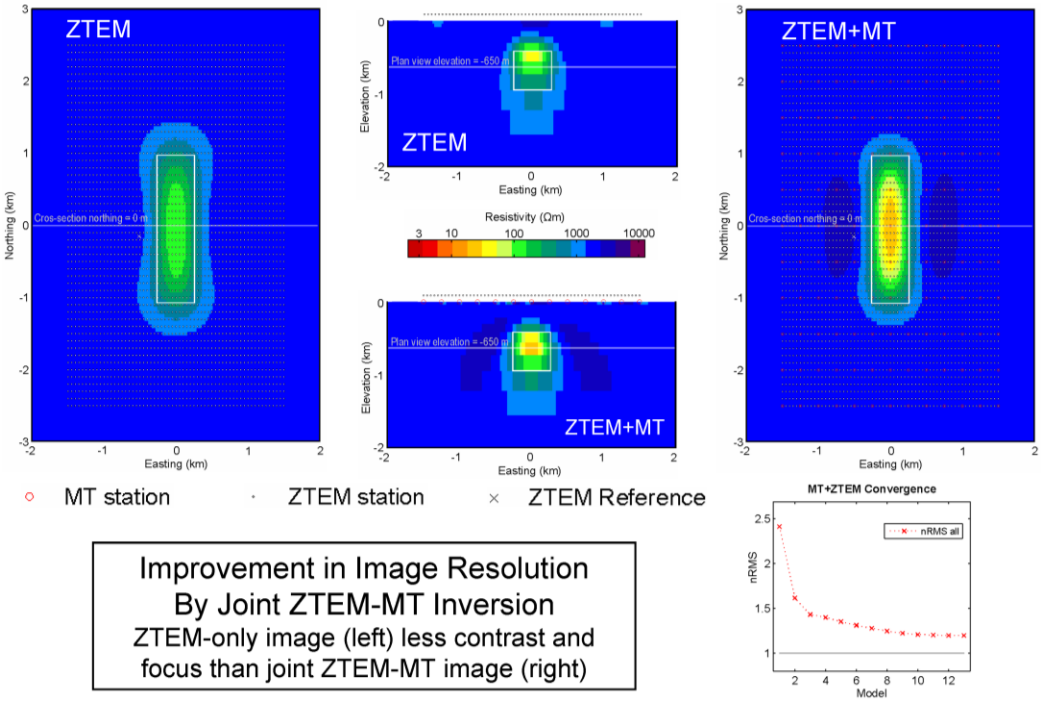

Figure 3: Synthetic joint ZTEM/MT inversion of 50 ohm-m prism in 2000 ohm-m background.

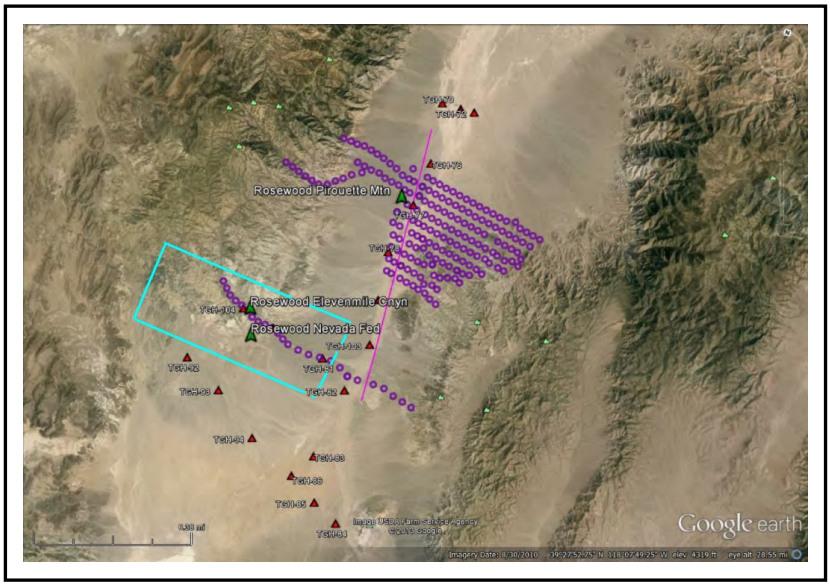

Figure 4: Google Earth view of MT and ZTEM data set coverage over the Eleven Mile Canyon geothermal area, Nevada. Light blue rectangle denotes the ZTEM footprint. Figure from MT contractor report provided by U.S. Navy (A. Sabin, PoC).

ELEVEN MILE CANYON 3D ZTEM AND MT DATA SET

Subsequently, the algorithm was applied to ZTEM and MT field data acquired over the Eleven Mile Canyon geothermal area in western Nevada (Lazaro et al., 2011) (Figure 4). MT and ZTEM data for the prospect was obtained from the respective contractors (Quantec Inc., Geotech Inc.) with approval of the U.S. Navy client. A 3D model of solely the ZTEM data was published by Devriese et al (2012). A single profile of MT data lies within the ZTEM coverage, extending to the ESE outside the ZTEM survey coverage (Figure 4). Although the profile form of the sparse MT coverage is not ideal, and would more desirably be as a scattered shotgun pattern, it serves to demonstrate the potential of the joint data set.

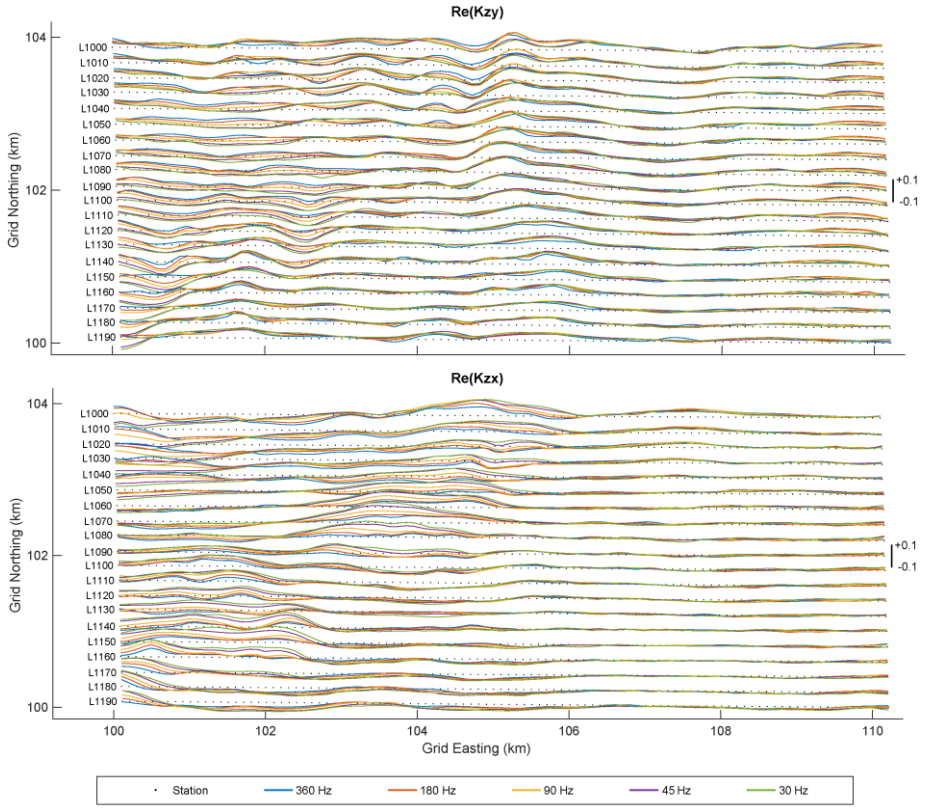

Figure 5: Example profile plots of ZTEM responses at five frequencies over the Eleven Mile Canyon geothermal area, Nevada.

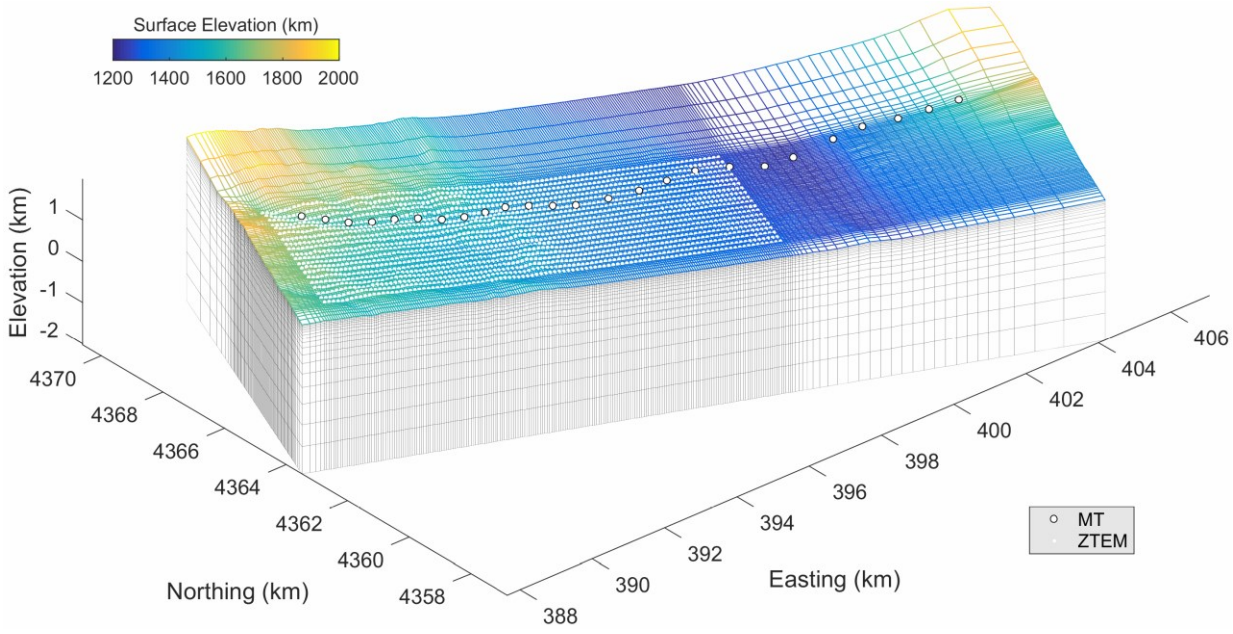

Figure 6: Google Earth view of MT and ZTEM data set coverage over the Eleven Mile Canyon geothermal area, Nevada. The light blue rectangle denotes the ZTEM footprint. Figure from MT contractor report provided by U.S. Navy.

Quality of ZTEM data delivered by the contractor appears good (Figure 5). For the inversion there are 2040 ZTEM stations in 20 flight profiles with 200 m separation. Along the lines, we have taken 100 m data intervals with five frequencies from 360 Hz – 30 Hz (40800 data). The mesh is 117 (x) x 261 (y) x 40 (z) nodes with 13 air layers (Figure 6); bird heights (62 – 179 m) are included. A 25 station MT profile onlapping from the east has 13 frequencies from 200 – 0.78 Hz (3120 data, upweighted by factor of 4). An impedance error floor of 0.1*[|Zxy-Zyx|/2] was applied to the MT, the ZTEM data error floor was 0.01 and the starting model was 100 ohm-m. Computations took ~5 hours/iteration on our 24 core, 0.5 TB RAM workstation.

For ZTEM-only inversion, model convergence was rapid and normalized root-mean-square (nRMS) data-model misfit reached 0.5 despite the small error floor of 0.01. An example data fit at 45 Hz appears in Figure 7. The model shows a possible clay alteration zone for depths just over 400 m but resolution degrades for depths much below that (Figure 8). There is a sharp transition from basement rocks to alluvium from west to east. This model compares favorably with the 3D ZTEM model published by Devriese et al (2012).

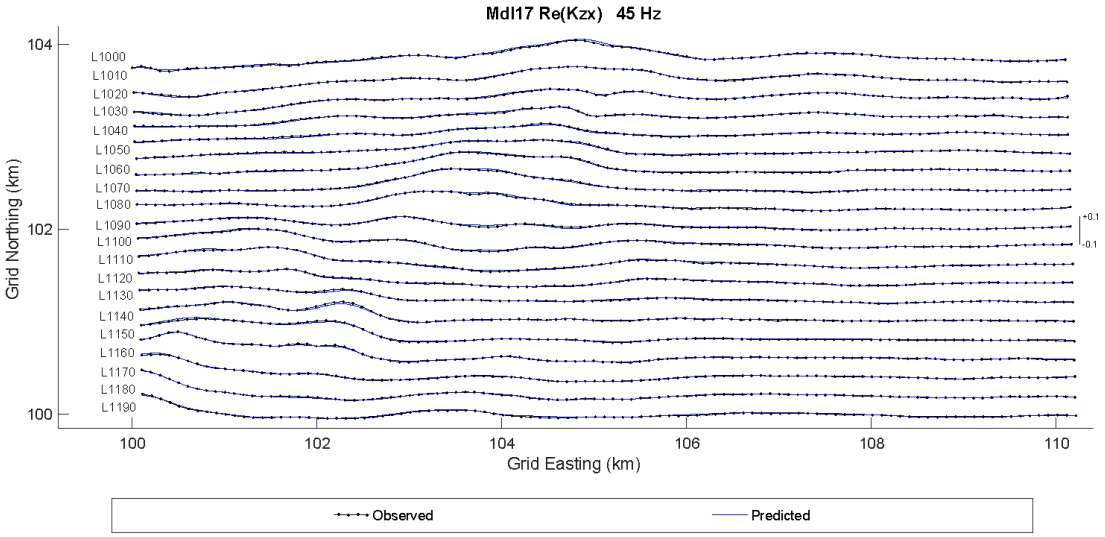

Figure 7: Example data model fit for data component Re(Kzx) (the non 2D component) of the ZTEM responses at 45 Hz over the Eleven Mile Canyon geothermal area, Nevada.

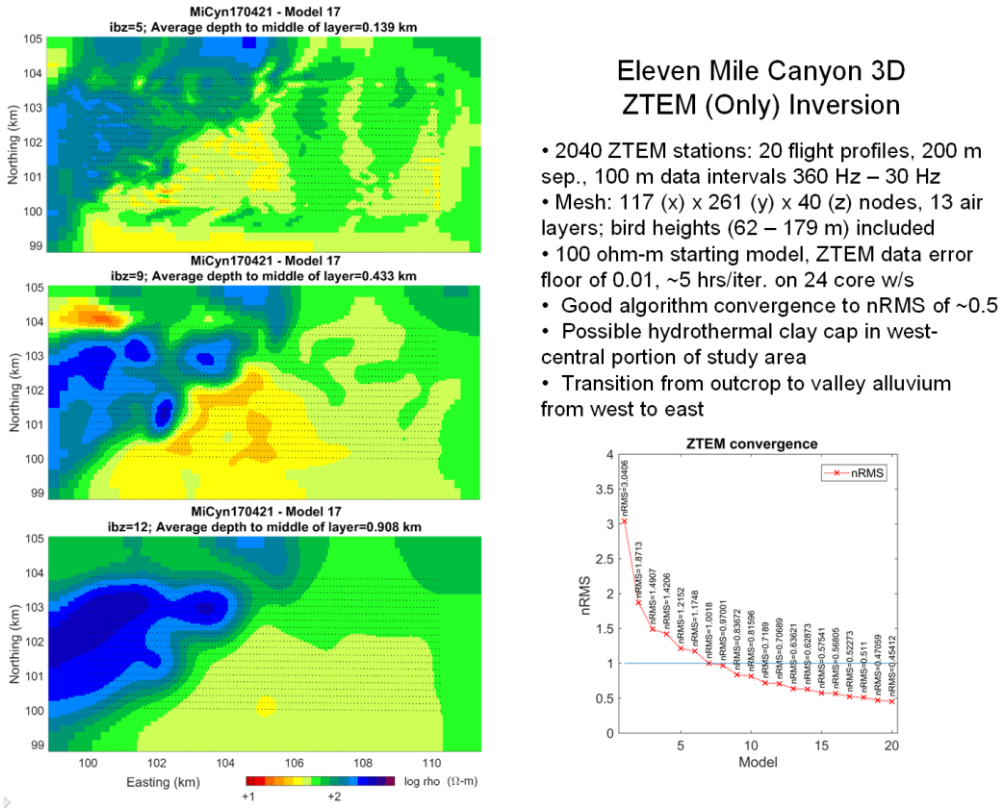

Figure 8: Resistivity inversion model for ZTEM responses at the Eleven Mile Canyon geothermal area, Nevada.

The resulting resistivity model and misfit convergence for joint ZTEM/MT inversion appears in Figure 9. One sees sharper definition along the possible hydrothermal alteration in the west-central portion of the survey area (Lazaro et al., 2011). There also is improved definition of the central graben and flanking resistive basement. This enhancement in imaging is interpreted to reflect better absolute resistivities possible by using the electric field of the MT data, plus the lower frequency range that comes with the MT.

One curious feature of this study is how the final nRMS fell to significantly less than unity for both ZTEM-only and joint ZTEM-MT. For the MT, this might indicate that the 10% error floor was too pessimistic. That the error floor of 0.01 on the ZTEM data was too low seems a stretch, however, because typical error floors assumed for related MT tipper data are of order 0.03. A close reading of the contractor report for the ZTEM survey indicated that the provided responses had been significantly smoothed laterally using a proprietary algorithm invoking both linear and non-linear filtering as a treatment for data noise. However, such a procedure would lead to a data set whose uncertainties very likely are not represented by a Gaussian probability distribution, which almost all inversion algorithms including ours assume explicitly in defining the parameter step and convergence criteria. The smoothing imposed on the ZTEM data made it "easier" to fit in the inversion process and led to the nRMS values falling well below unity even assuming a small error floor (0.01).

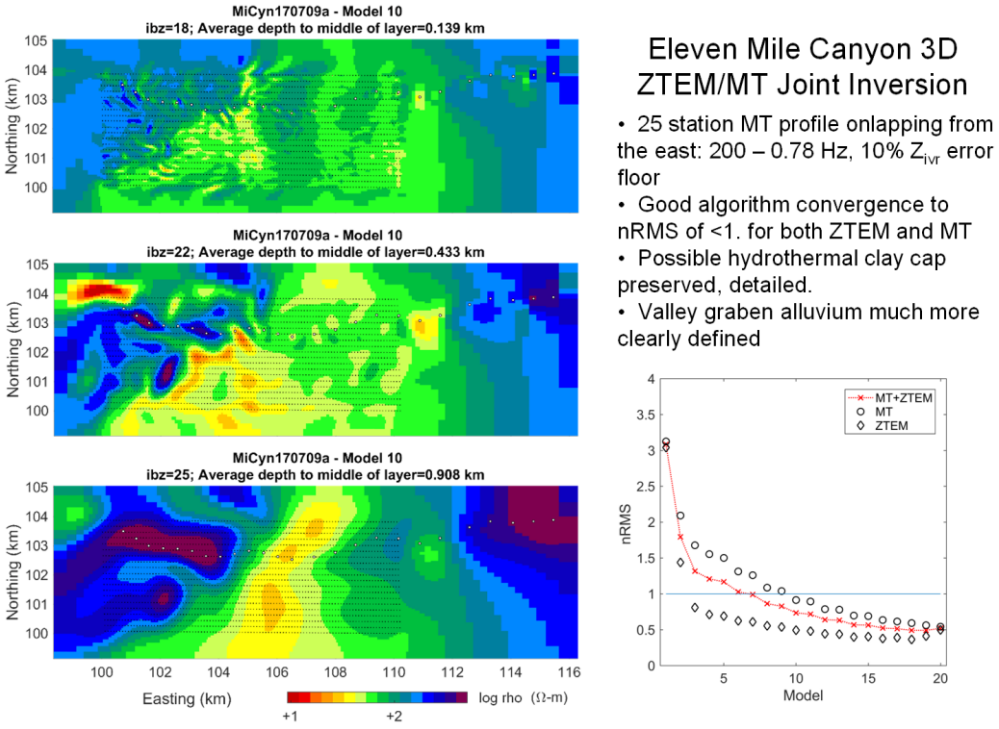

Figure 9: Resistivity inversion model for ZTEM responses at the Eleven Mile Canyon geothermal area, Nevada.

We subsequently received from the contractor a version of the Eleven Mile Canyon ZTEM data set which had not been subject to lateral filtering/smoothing. An example of the raw data at its original ~10 m sampling interval is shown for two frequencies in Figure 10 underlain by its smoothed counterpart. The character is more typical of expected unfiltered data, with a random noise aspect added to longer distance trends plus a limited number of large spikes.

In an attempt to suppress random noise and define a data set with lateral sampling that is comparable to flight height and expected resolving scales, the data were filtered with a "hat" function 100 m wide. The results appear in Figure 11 (middle). These show a similar character to the smoothed results but with local randomness as expected. It also is apparent that occasional large spikes are not sufficiently suppressed by simple lateral averaging. In an attempt at simple outlier removal, data values with magnitudes exceeding 0.5 were replaced by zeroes, which is the expected ZTEM response value in the absence of heterogeneity, and re-averaged using the hat function. This had a positive effect on the response curves (Figure 11, bottom) and they appear as expected for good quality data with limited statistical uncertainty.

The laterally averaged data after spike removal have been inverted using the joint algorithm described previously and the resulting model plotted in Figure 12 at three depth levels. Now, the nRMS plots show monotonic convergence to values near unity for both MT and ZTEM. The resolution of alteration and graben structure appear to be the best of the models so far. We consider this to be the superior result of our efforts in this area. Methods of outlier removal more sophisticated than the simple spike removal applied here, such as jackknifing (e.g., Thompson and Chave, 1991; Wannamaker et al., 2004). could improve the statistics of ZTEM data further. At this point we consider that to be beyond the scope of the current project.

Fits of the 3D model to the MT profile data are shown in Figure 13. The computations appear to underfit the data to a modest extent, presumably an effect of the smoothing regularization which is intended to produce a conservative model. However, given that the MT component of the nRMS also falls to just below unity then the apparent underfit is not statistically significant. As seen by the relatively high values of xy and yx impedance phase at the shorter periods (0.1 – 0.005 s, or 10-200 Hz), a prominent structure is the central graben alluvium. Concentrated features in the west-central part of the profile denote possible flanking alteration zones as mentioned previously (Lazaro et al., 2011).

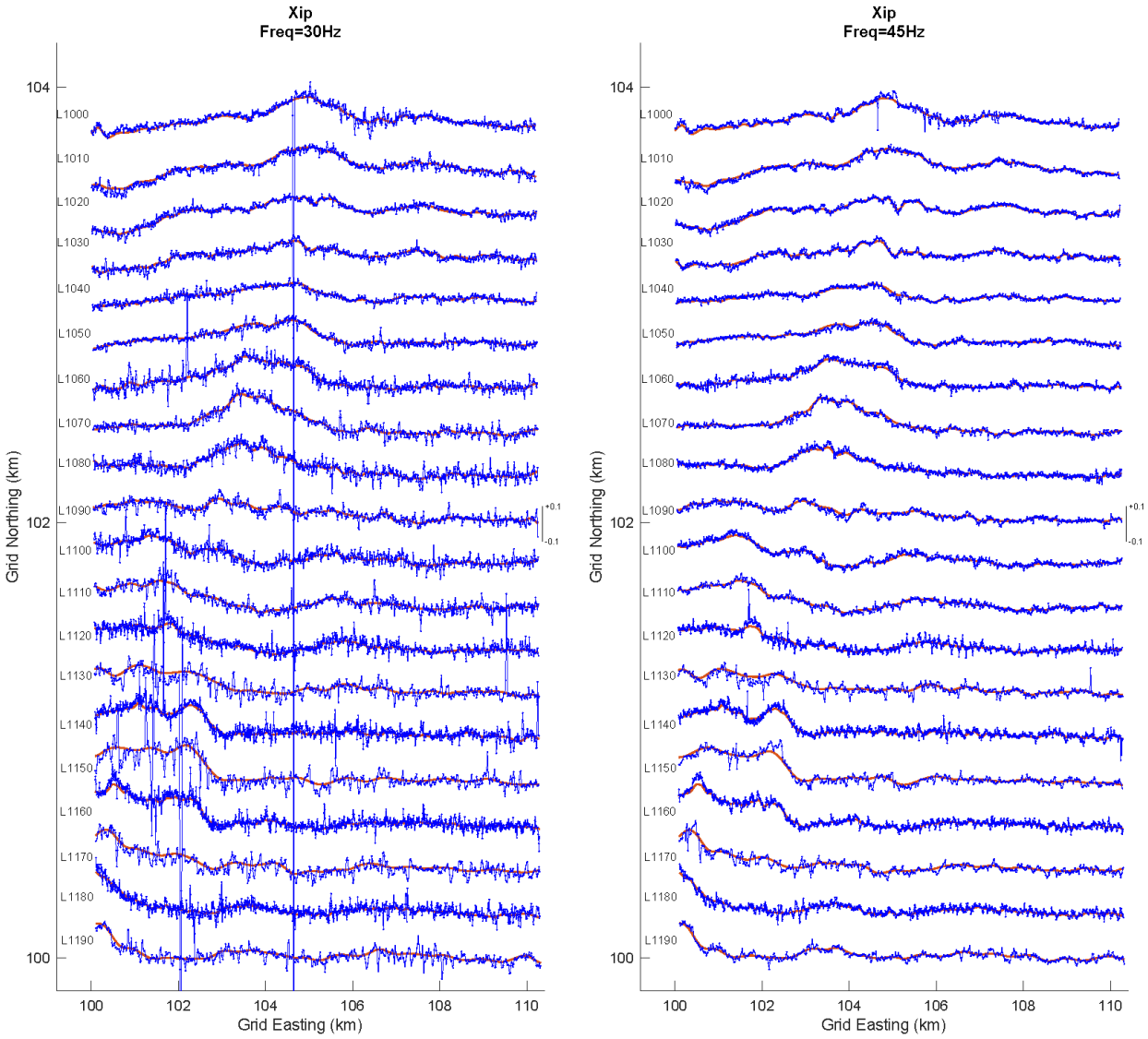

Figure 10: Resistivity inversion model for ZTEM responses at the Eleven Mile Canyon geothermal area, Nevada.

CONCLUSIONS

ZTEM ambiguities may be reduced through formal incorporation with possibly sparse ground MT soundings, which has been demonstrated herein using both synthetic and field data sets. Separate and joint 3D resistivity inversion models were carried out for the donated Eleven Mile Canyon MT-ZTEM data set to demonstrate concept. ZTEM only inversion showed two main alteration zones in the western portion of the project area known from geological mapping. Joint inversion including an E-W profile of MT soundings sharpened these features considerably. It also resolved in much greater detail the graben related normal faulting structure of the central project area which lies at depths exceeding the sensitivity of ZTEM alone. The sparse number of MT data relative to the ZTEM required upweighting the former by a factor of several in order to achieve similar joint data misfits. However, this amount is much lower than the ratio between number of ZTEM and MT data points, which typically is 25-50. Future research might pursue the relative contributions of the data types to the inversion model update (step), which involves not just the number of data but also the relative parameter-data sensitivities. Our final impression is that sparse MT data can improve resolution of the subsurface over that of ZTEM alone. However, if logistically feasible, well sampled MT data may be preferred by offering the simplicity of interpreting just one data type, by possessing potentially superior resolution capability coming with having the electric field everywhere, and from their substantial bandwidth.

ACKNOWLEDGEMENTS

We wish to thank Larry Petrie, Denison Mines Corp., for providing the Johnston Lake ZTEM and MT data sets, and Andy Sabin, U.S. Navy, for providing the Eleven Mile Canyon ZTEM and MT data sets. This work was supported initially in a cooperative DOE/GTO/AOP project (Contract No. 89233218CNA000001) with Los Alamos National Laboratory and Lawrence Livermore National Laboratory under LLNL contract B616897 to Wannamaker. Subsequently it was supported under DOE/GTO contract DE-EE0007697 to Wannamaker. We thank Dr. Michal Kordy for his assistance in implementing ZTEM data analysis with algorithm HexMT.

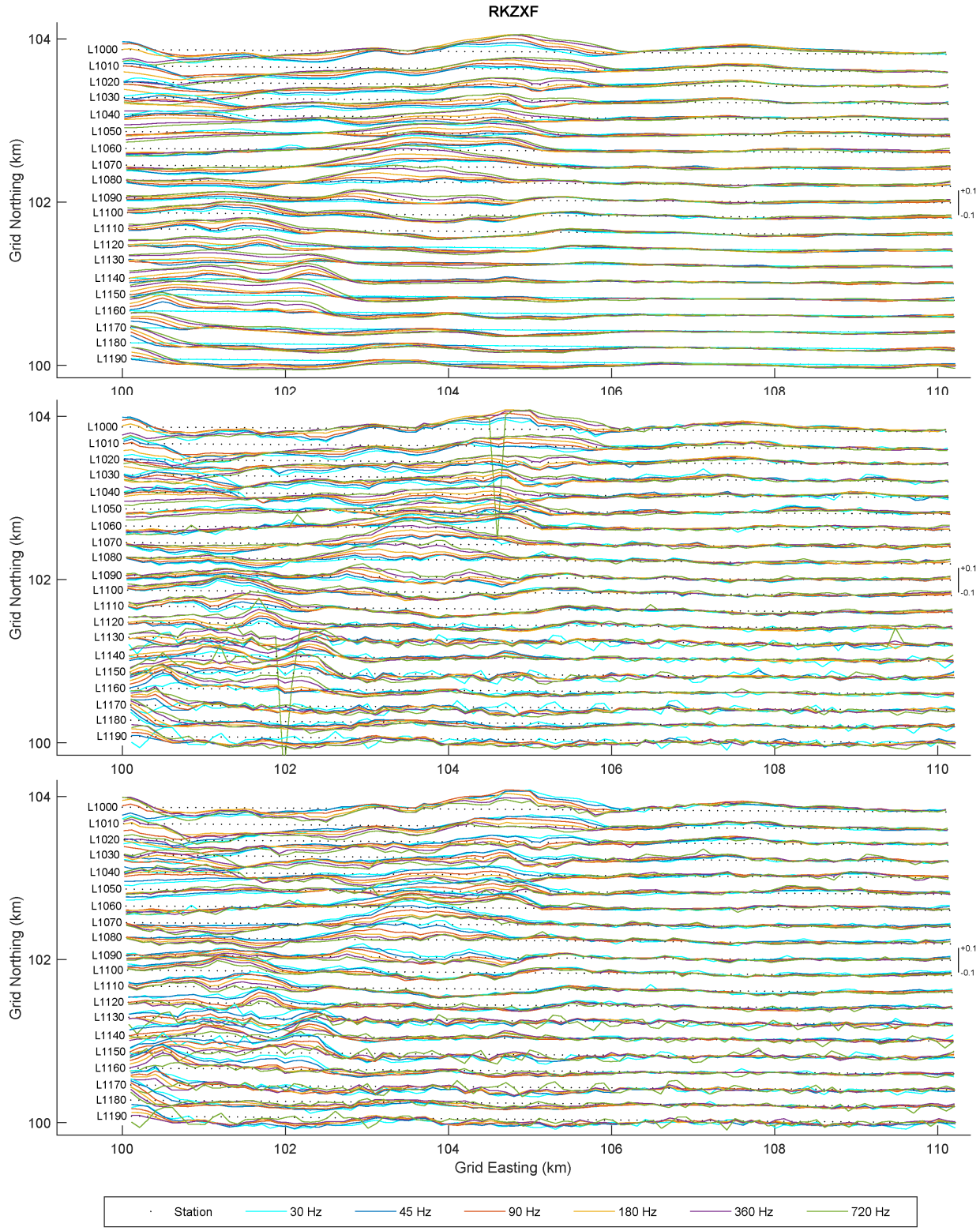

Figure 11: Contractor-smoothed (top), hat-averaged before spike removal (middle) and hat-averaged after spike removal (lower) ZTEM X-component (east) in-phase response components at all six frequencies for the Eleven Mile Canyon survey area. Note, statistics cannot be derived for the uppermost smoothed responses with current information.

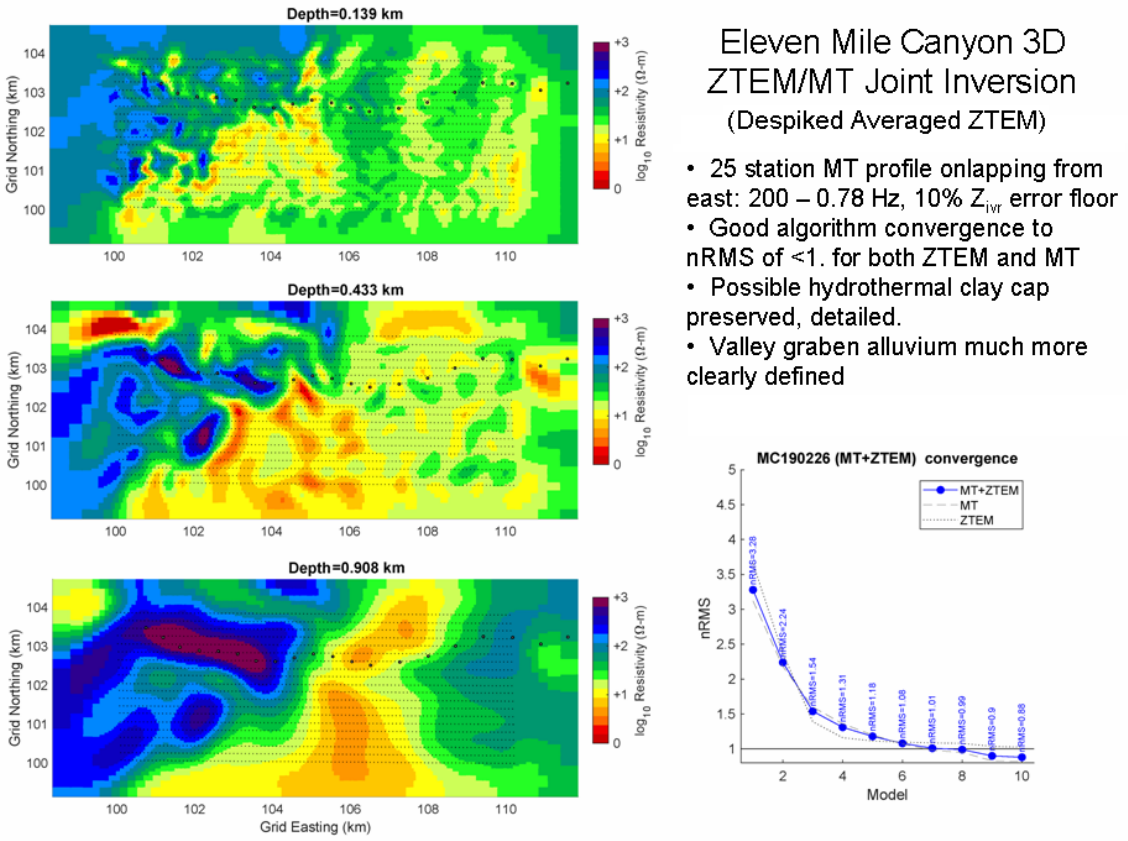

Figure 12: Resistivity inversion model for joint ZTEM/MT responses at the Eleven Mile Canyon geothermal area, Nevada, using unsmoothed ZTEM data subject to simple outlier removal and lateral "hat" averaging.

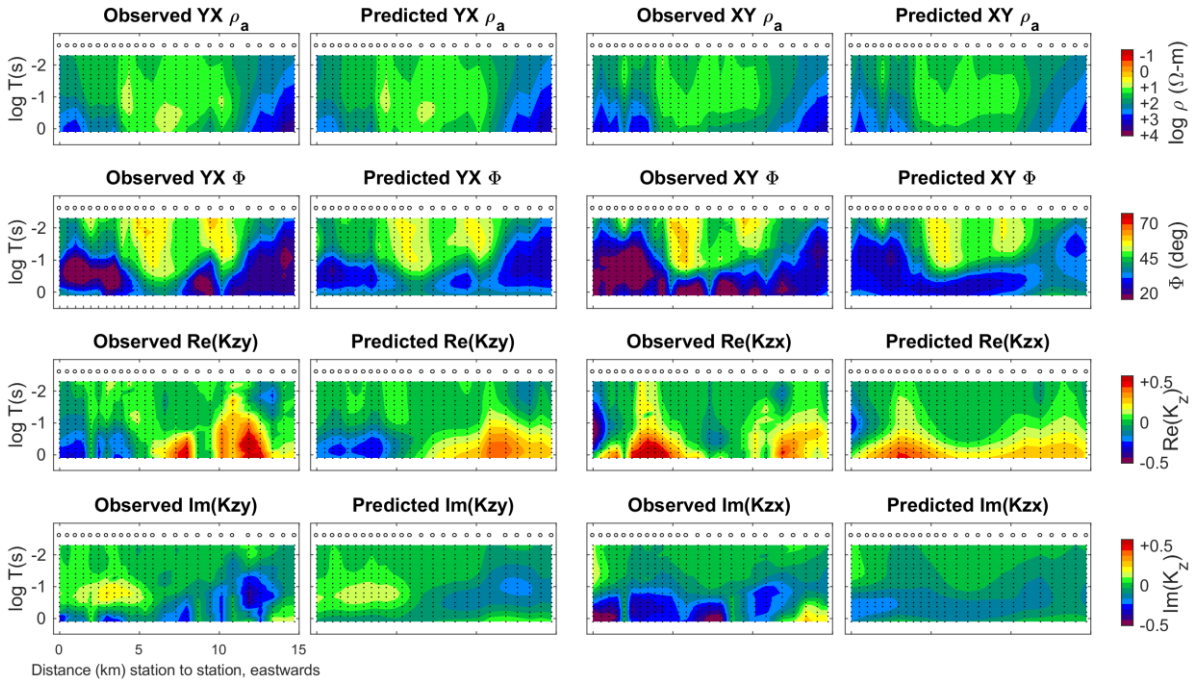

Figure 13: Apparent resistivity and impedance phase pseudosections for observed and predicted MT profile data across Eleven Mile Canyon geothermal prospect, Nevada. X axis of data definition is N020.

REFERENCES

Chave, A. D., and A. G. Jones, eds, The magnetotelluric method: theory and practice: Cambridge University Press, New York, 570 pp., 2012.

Devriese, S. G. R., D. W. Oldenburg, and J. D. Shoffner, Three-dimensional inversion of ZTEM data at the Eleven Mile Canyon geothermal system, Nevada: Geothermal Resource Council Transactions, 36, 995-1000, 2012.

Holtham, E., and D. W. Oldenburg, Three-dimensional inversion of ZTEM data: Geophysical Journal International, 182, 168-182, 2010.

Kelbert, A., N. Meqbel, G. D. Egbert, and K. Tandon, ModEM: a modular system for inversion of electromagnetic geophysical data: Computers & Geosciences, 66, 40-53, 2014.

Kordy, M. A., P. E. Wannamaker, V. Maris, E. Cherkaev, and G. J. Hill, Three-dimensional magnetotelluric inversion using deformed hexahedral edge finite elements and direct solvers parallelized on SMP computers, Part I: forward problem and parameter jacobians: Geophysical Journal International, 204, 74-93, 2016a.

Kordy, M. A., P. E. Wannamaker, V. Maris, E. Cherkaev, and G. J. Hill, Three-dimensional magnetotelluric inversion using deformed hexahedral edge finite elements and direct solvers parallelized on SMP computers, Part II: direct data-space inverse solution: Geophysical Journal International, 204, 94-110, 2016b.

Lazaro, M., S. Alm, A. Tiedeman, C. Page, D. Meade, J. Shoffner and K. Bucher, Department of the Navy geothermal exploration on Naval Air Station Fallon (NASF) managed lands in Dixie Valley, Nevada: Geothermal Resource Council Transactions, 35, 873-878, 2011.

Lee, B. M., M. J. Unsworth, J. Hubert, J. P. Richards J. M. Legault, 3D joint inversion of magnetotelluric and airborne tipper data: a case study from the Morrison porphyry Cu–Au–Mo deposit, British Columbia, Canada: Geophysical Prospecting, 66, 397–421, doi: 10.1111/1365-2478.12554, 2018.

Legault, J. M., H. Kumar, B. Milicevic, and P. Wannamaker, ZTEM tipper AFMAG and 2D inversion results over an unconformity uranium target in northern Saskatchewan: Expanded abstract, Society of Exploration Geophysicists Annual Meeting, Houston, 1277-1281, 2009.

Newman, G. A., and D. L. Alumbaugh, Three-dimensional magnetotelluric inversion using non-linear conjugate-gradients: Geophys. J. Int., 140, 410-424, 2000.

Phillips, B., J. Ziagos, H. Thorsteinsson, and E. Hass, A roadmap for strategic development of geothermal exploration technologies: Proc. 38th Workshop on Geothermal Reservoir Engineering, SGP-TR-198, Stanford University, Stanford, California, February 11-13, 12 pp., 2013.

Siripunvaraporn, W., G. Egbert, Y. Lenbury, and M. Uyeshima, Three-dimensional magnetotelluric inversion: data-space method: Phys. Earth Planet. Inter., 150, 3-14, 2005.

Thompson, D. J., and A. D. Chave, Jackknifed error estimates for spectra, coherences, and transfer functions: in Advances in Spectrum Analysis and Array Processing, ed. Haykin, S., Prentice Hall, Englewood Cliffs, 58–113, 1991.

Wannamaker, P. E., and J. M. Legault, Two-dimensional joint inversion of ZTEM and MT plane-wave EM data for near surface applications: Proc. 27th Symposium on the Application of Geophysics to Engineering and Environmental Problems (SAGEEP), Boston, MA, March 16-20, 134-139, doi: 10.4133/SAGEEP.27-013, 2014.

Wannamaker, P. E., J. A. Stodt, L. Pellerin, S. L. Olsen, and D. B. Hall, Structure and thermal regime beneath South Pole region, East Antarctica, from magnetotelluric measurements: Geophysical Journal International, 157, 36-54, 2004.

Wannamaker, P. E., D. P. Hasterok, J. M. Johnston, J. A. Stodt, D. B. Hall, T. L. Sodergren, L. Pellerin, V. Maris, W. M. Doerner, and M. J. Unsworth, Lithospheric dismemberment and magmatic processes of the Great Basin-Colorado Plateau transition, Utah, implied from magnetotellurics: Geochemistry, Geophysics, Geosystems, 9, Q05019, doi:10.1029/ 2007GC001886, 2008.

Wannamaker, P. E., G. Hill, J. Stodt, V. Maris, Y. Ogawa, K. Selway, G. Boren, E. Bertrand, D. Uhlmann, B. Ayling, A. M. Green and D. Feucht, Uplift of the Central Transantarctic Mountains: Article, Nature Communications, doi: 10.1038/s41467-017-01577-2, 11 pp., 2017.

Wannamaker, P. E., J. E. Faulds, B. M. Kennedy, V. Maris, D. L. Siler, C. Ulrich, and J. N. Moore, Integrating magnetotellurics, soil gas geochemistry and structural analysis to identify hidden, high enthalpy, extensional geothermal systems: Proc. 43rd Workshop Geothermal Reservoir Engineering, Stanford University, Stanford, CA, SGP-TR-214, 19 pp., 2019.

Wannamaker, P., V. Maris, K. Mendoza and J. Moore, Deep Heat and Fluid Sources for Roosevelt Hot Springs Hydrothermal System and Potential Heat for the Utah FORGE EGS from 3D FORGE and SubTER Magnetotelluric Coverage: Geothermal Resource Council Transactions, 45, 847-863, 2021.

Ziagos, J., B. Phillips, L. Boyd, A. Jelacic, G. Stillman, and E. Hass, A technology roadmap for strategic development of enhanced geothermal systems: Proc. 38th Workshop on Geothermal Reservoir Engineering, SGP-TR-198, Stanford University, Stanford, California, February 11-13, 24 pp., 2013.